The Planetary Science Journal, 4:205 (9pp), 2023 November https://doi.org/10.3847/PSJ/ad0040

Infrared Spectra and Vapor Pressures of Crystalline C_2N_2, with Comparisons to Crystalline HCN

Reggie L. Hudson and Perry A. Gerakines
Astrochemistry Laboratory, NASA Goddard Space Flight Center, Greenbelt, MD 20771, USA; reggie.hudson@nasa.gov
Received 2023 April 24; revised 2023 September 13; accepted 2023 September 27; published 2023 November 2

Abstract

In a continuation of our work on nitriles, we have examined cyanogen (C_2N_2) as a crystalline solid, comparing the results to our recent work on crystalline hydrogen cyanide (HCN). A density and refractive index for C_2N_2 ice were measured and used to prepare solid samples from which infrared (IR) spectra, band strengths, and optical constants were measured. The vapor pressures (sublimation pressures) of both C_2N_2 and HCN ices were determined with a quartz-crystal microbalance at temperatures relevant to Titan's atmosphere and much lower than those in the literature. Comparisons of the newly measured low-temperature vapor pressures to values extrapolated from higher temperatures revealed differences on the order of 45 and 130%. The enthalpies of sublimation of C_2N_2 and HCN in the 120 K region were measured and found to be similar to those at higher temperatures. Comparisons were made to previous spectroscopic work, but hindered in the case of IR intensities by the lack of published details.

Unified Astronomy Thesaurus concepts: Titan (2186); Astrochemistry (75); Experimental techniques (2078)

1. Introduction

Nitriles are molecules with a −C≡N: functional group, and are found within and beyond the solar system. The cyano radical (CN) can be taken as the simplest nitrile, and has long been observed as a component of cometary comae. Among the simpler nitriles is cyanogen (C_2N_2), which has been identified in comets along with hydrogen cyanide (HCN), acetonitrile (CH_3CN), and cyanoacetylene (HCC-CN); see Hänni et al. (2021). Cyanogen also is known in the interstellar medium (ISM) through its conjugate acid, $HC_2N^+_2$ (Agúndez et al. 2015). Members of the homologous series H–$(C\equiv C)_x$–C≡N:, with x = 0–5, have been identified in the ISM by radio observations in the gas phase (e.g., Loomis et al. 2021), as have various unsaturated nitriles, nitrile isomers, the nitrile ion OCN^-, known as cyanate, and two aromatic nitriles (Soifer et al. 1979; Lovas et al. 2006; McGuire et al. 2018, 2020; Sita et al. 2022).

The N_2 + CH_4 atmosphere of Titan is relatively rich in nitriles, with evidence for at least seven in the literature (i.e., HCN, C_2N_2, CH_3CN, CH_3CH_2CN, HCCCN, C_2H_3CN, and C_4N_2), with identifications coming from both ground- and space-based observations as well as in situ measurements (e.g., Kunde et al. 1981; Khanna et al. 1987; Lai et al. 2017). Such identifications and associated analyses rely heavily on laboratory measurements, to which we have contributed. For example, in Moore et al. (2010) we examined HCN, C_2N_2, CH_3CN, C_2H_5CN, and HC_3N, returning with new data to HCN, CH_3CN, and C_2H_5CN in later papers (Hudson 2020; Gerakines et al. 2022).

In this paper, we focus on crystalline C_2N_2. We describe measurements of infrared (IR) intensities, comparing and contrasting with our recent work on HCN. For this, we required determinations of a reference density and refractive index for C_2N_2 ice, which we also report here. Finally, we describe the first vapor-pressure measurements of solid C_2N_2 and solid HCN in the 100–140 K region, lower than in previous papers and specifically chosen for applications to Titan's atmosphere.

2. Laboratory Procedures

Details of our experimental procedures and equipment are in print, and so only a summary is given here; see, for example, Moore et al. (2010) or Hudson et al. (2020) for additional information.

Our C_2N_2 was from Matheson and contained ∼0.2% HCN, along with trace amounts of H_2O and CO_2 (< ∼0.01%). No attempt was made to remove these impurities as the levels involved were insufficient to cause detectable changes in either vapor pressures or IR band strengths within the accuracy and sensitivity of our measurements. Our HCN was synthesized by the reaction of potassium cyanide and stearic acid as in earlier papers (Gerakines et al. 2004, 2022). *Caution*: Both HCN and C_2N_2 are highly toxic and should be used only by experienced personnel.

Crystalline ices were prepared by gas-phase deposition of either C_2N_2 or HCN onto a precooled CsI substrate in a vacuum chamber (∼10^{-8} Torr). The condensation rate of the room-temperature gases was such as to give an increase in the resulting ice's thickness of 3–4 μm hr^{-1}. Spectra were recorded with a Thermo iS50 spectrometer at resolutions from 2 up to 0.125 cm^{-1}, but mainly at 1 and 0.5 cm^{-1}, over about 3000–500 cm^{-1} for C_2N_2 and about 5000–500 cm^{-1} for HCN with 200 accumulations per spectrum.

Earlier laboratory work suggested that a temperature of 90 K was sufficient to crystallize amorphous cyanogen on warming from lower temperatures, and that 100 K was a reasonable estimate for C_2N_2 condensation in Titan's atmosphere (Coustenis et al. 1999); see also later work on condensation by Lai et al. (2017), Anderson et al. (2018), and Bézard et al. (2018). Therefore, our cyanogen ices were grown at 100 K and held there for recording spectra. The IR spectra of such ices were essentially identical to those of crystalline C_2N_2 found in the literature (vide infra).

Infrared band strengths, denoted A' (in cm molecule^{-1}) were obtained in the usual manner by integrating an IR band of interest in the spectrum of an ice of known thickness (Hollenberg & Dows 1961). Several such integrations with ices of different thicknesses were plotted to give a Beer's law curve in accord with Equation (1):

$$\int_{\text{band}} (\text{Absorbance})\, d\tilde{\nu} = \left(\frac{\rho_N A'}{\ln(10)}\right) h. \quad (1)$$

In Equation (1), h is the ice thickness in cm, ln(10) converts the absorbance spectrum (common logarithm base) to an optical-depth scale (natural logarithm base), and ρ_N is the number density (molecules cm^{-3}). The latter was calculated from ice densities as $\rho_N = \rho\ (N_A/M)$, where M is the molar mass (g mole^{-1}) of the compound studied, ρ (in g cm^{-3}) is mass density, and N_A is Avogadro's constant (molecules mole^{-1}). Each plot of the left-hand side of Equation (1) as a function of h possessed a slope ($\rho_N\, A'/\ln(10)$) from which A' was calculated. All such Beer's law plots had correlation coefficients of 0.998 and higher; see our earlier papers for examples of the same method (e.g., Gerakines & Hudson 2015).

Our usual method for determining ice thickness is to record interference fringes during the growth of an ice; see, for example, our previous work with HCN (Gerakines et al. 2022). However, the IR features of C_2N_2 were so weak that the initially uniform pattern of fringes was lost before ices were sufficiently thick to show IR bands intense enough for reliable integration. Therefore, thicknesses for crystalline cyanogen were found from the smooth, regular pattern of channel fringes in the ice's IR spectrum. For N_{fr} channel fringes observed over a wavenumber interval $\Delta\tilde{\nu}$, the sample's thickness was just $N_{\text{fr}}/(2\ n_{670}\ \Delta\tilde{\nu})$; see, as examples, either Harrick (1971), Griffiths & de Haseth (1986), or Ospina et al. (1988). In all cases, a refractive index (n_{670}) was needed to determine an ice thickness and an ice density was required to calculate a band strength with Equation (1). The required refractive indices and ice densities (ρ) were measured in an ultra-high vacuum (UHV) chamber ($\sim 10^{-10}$ Torr). Two-laser interferometry gave n_{670} and microgravimetry with a quartz-crystal microbalance (QCM) gave ρ (Tempelmeyer & Mills 1968; Lu & Lewis 1972).

Again, the experimental techniques employed resembled those used in our laboratory and elsewhere for many years. Readers unfamiliar with these methods might wish to consult some of our earlier papers such as Moore et al. (2010), Hudson et al. (2020), or Gerakines et al. (2022), and references therein.

3. Results

3.1. Density and Refractive Index

Our measurements of the refractive index and density of crystalline HCN at 120 K were reported in Gerakines et al. (2022). We were unable to find comparable values for cyanogen, so they were measured in our UHV chamber. The result for crystalline C_2N_2 at 100 K was $n_{670} = 1.462 \pm 0.003$ and $\rho = 1.186 \pm 0.005$ g cm^{-3} as averages and standard errors from five determinations. The angles of the two lasers in our UHV chamber are known to three significant figures, but an extra number has been retained in these n_{670} and ρ results. Rounding can be done as desired. We return to these n_{670} and ρ values in our Discussion (see Section 4).

3.2. Infrared Spectra of Ices

Our recent results for HCN (Gerakines et al. 2022) provide a convenient comparison to the new work on C_2N_2 presented here, and are so used. The IR spectra of hydrogen cyanide and cyanogen are quite different. With three atoms in a linear arrangement, HCN has 3N–5 = 3(3)–5 = 4 fundamental vibrations, each being both IR and Raman active. All can be seen in the upper trace of Figure 1, with the IR feature near 826 cm^{-1} being a doubly degenerate bending mode. This spectrum is of an ice with a column density of about 1.1×10^{18} HCN molecules cm^{-2}. Table 1 gives band positions and intensities (i.e., A') from Gerakines et al. (2022).

Cyanogen is a four-atom linear molecule, but its center of symmetry means that it is nonpolar and that there are no vibrations that are both IR and Raman active in the gas and crystalline phases. Its 3N–5 = 3(4)–5 = 7 fundamental vibrations include just three that are IR active, an asymmetric C≡N stretching mode near 2165 cm^{-1} and a doubly degenerate bending near 240 cm^{-1}, which is beyond the range we studied. Table 2 summarizes the activity and positions of the fundamental vibrations of crystalline C_2N_2 (Andrews et al. 1984). Note that our description of the ν_2 vibration differs from that in the compilation of Shimanouchi (1972) due to a typographical error in the latter.

Crystalline cyanogen is unusual in being composed of polyatomic molecules with but one fundamental vibration in the mid-infrared (mid-IR) region. The spectrum of crystalline C_2N_2 ice at 100 K is shown in Figure 2, with the three labeled transitions being the strongest bands from 5000 to 300 cm^{-1}, and the main cyanogen features examined for this study. Each of the three bands of Figure 2 consists of a small and large component, as expected from the theory of vibrations in crystalline solids (e.g., Verderame et al. 1963). As for intensities, even a casual comparison of the ice thicknesses and peak heights in Figures 1 and 2 shows that C_2N_2 is a particularly weak IR absorber compared to HCN.

With Equation (1) in mind, the IR spectra of nine crystalline C_2N_2 ices at 100 K with thicknesses from about 0.7×10^{-4} to 5×10^{-4} cm (0.7 to 5 μm) were recorded and the three bands in Figure 2 integrated for each ice sample. Plots of the integrals as a function of thickness were linear (correlation coefficients >0.998) and gave slopes from which band strengths (A') were calculated. Table 3 summarizes the results. Note that a resolution of 1 cm^{-1} was used to record the IR spectra of Figures 1 and 2, and for the data leading to Tables 1 and 3, higher resolutions (e.g., 0.5 cm^{-1}) giving essentially the same results. Our resolutions bracketed the 0.6 cm^{-1} used by Ospina et al. (1988).

The uncertainties in our A' values are mainly due to the determination of cyanogen ice thicknesses, which depended on the n_{670} we measured. The fact that we were able to measure n_{670} to a reasonably high accuracy, coupled with the relative sharpness of the three IR bands examined and the lack of interference from overlapping features, enabled thickness uncertainties to be lowered from the ∼25% of Ospina et al. (1988) to about 2%. A propagation-of-errors approach and a least-squares regression analysis with uncertainties in both the x- and y-axes of Beer's law plots (Irvin & Quickenden 1983; Press et al. 1992) was used to calculate an uncertainty of about 8% in A' for the $\nu_3 + \nu_4$ and ν_3 bands, and about 2% for the stronger $\nu_4 + \nu_6$ feature.

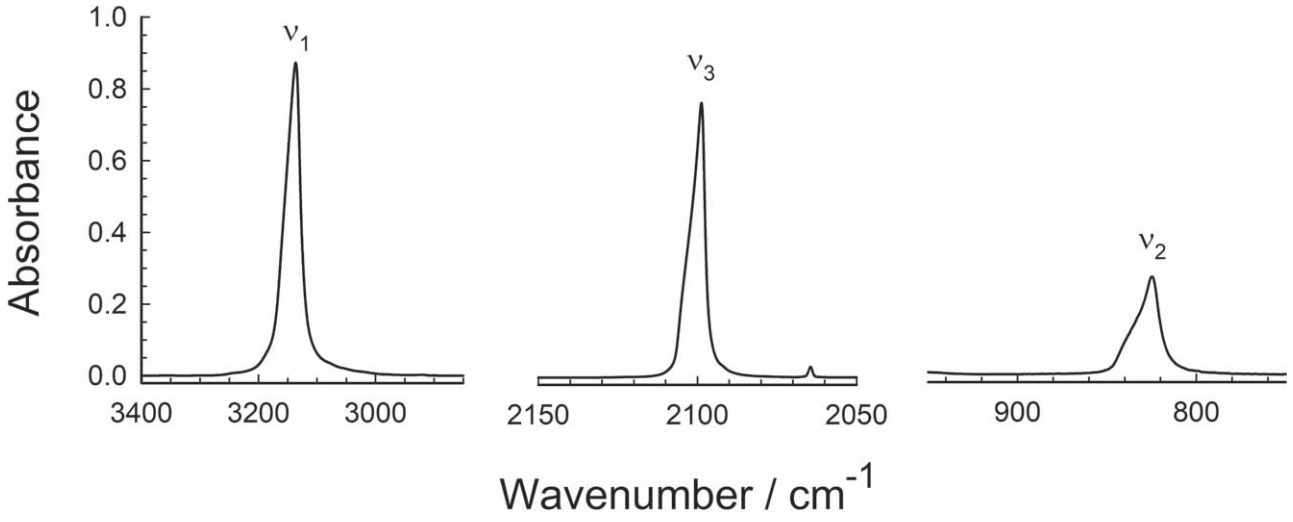

Figure 1. The three fundamental vibrational bands of crystalline HCN deposited and recorded at 120 K. The ice thickness was 0.47 μm = 0.47 × 10^{-4} cm (channel fringes removed for clarity); see also Gerakines et al. (2022).

Table 1
Fundamental Vibrations of Crystalline HCN at 120 K[a]

Assignment	Description	$\tilde{\nu}$/cm^{-1}	$A'/10^{-18}$ cm molecule^{-1}
ν_1	CH stretch	3136	70.30
ν_3	CN stretch	2099	10.28
ν_2	HCN bend	826	10.57

Note.
[a] Positions and intensities are from Gerakines et al. (2022). All vibrations are both IR and Raman active.

Table 2
Fundamental Vibrations of Crystalline C_2N_2 at 20 K[a]

Assignment	Description	Raman $\tilde{\nu}$/cm^{-1}	Infrared $\tilde{\nu}$/cm^{-1}
ν_1	CN s-stretch	2340	⋯
ν_3	CN a-stretch	⋯	2158
ν_2	CC stretch	850	⋯
ν_4	s-sym bend	508	⋯
ν_5	a-sym bend	⋯	244

Note.
[a] Positions are from Andrews et al. (1984). Splittings and substructure are seen for all but the ν_2 vibration. The ν_4 and ν_5 vibrations are doubly degenerate.

Having new IR spectra of C_2N_2 for ices of known thickness, it seemed reasonable to use these same spectra to calculate optical constants $n(\tilde{\nu})$ and $k(\tilde{\nu})$ for cyanogen at 100 K. Our method was the same as in Gerakines & Hudson (2020) using the open-source software described in that paper, which was developed by one of us (P.A.G.) and remains the only such free, open software for the planetary-science community. Infrared spectra used for these calculations were for crystalline C_2N_2 made, and spectra recorded, at 100 K with 1 cm^{-1} resolution. Figure 3 shows the results for the same three regions of our Figure 2; see https://science.gsfc.nasa.gov/691/cosmicice/constants.html or the Zenodo repository (doi:10.5281/zenodo.8335802) for our optical constants of crystalline cyanogen at 100 K.

3.3. Vapor Pressures of Ices

Vapor pressures are needed to determine the condensation height of atmospheric components of Titan and other worlds (e.g., Sagan & Thompson 1984), but the relevant laboratory data for both HCN and C_2N_2 are very limited. Lewis & Schutz (1934) reported vapor pressures for solid HCN at six temperatures, followed by Appleton & Van Hook (1982), who published a vapor-pressure curve for solid HCN at 237–256 K, based on 26 points. To these measurements can be added about 20 data points for solid C_2N_2 found in refereed publications, covering roughly 200–240 K (Perry & Bardwell 1925; Ruehrwein & Giauque 1939). Figure 4 summarizes the literature results for HCN and C_2N_2 and shows that the available vapor pressures are far above the ∼100–150 K region at which nitriles are expected to condense in Titan's atmosphere. The altitude of ∼200 km for 150 K in Figure 1 is from Anderson et al. (2018), but values closer to 150 km (Lai et al. 2017) or even 100 km (Bézard et al. 2018) can be found in the literature.

The lack of low-temperature vapor-pressure data for HCN and C_2N_2 has motivated extrapolations by several researchers to cover the temperature gap down to ∼120 K and lower, with accompanying pressure extrapolations over about five orders of magnitude; see Fray & Schmitt (2009) for a discussion of proposed extrapolations and curve fits. Here, we address this paucity of laboratory data by reporting vapor pressures of solid HCN and C_2N_2 between about 120 and 140 K for HCN and 105 and 120 K for C_2N_2.

Our method and equipment for vapor-pressure measurements have been described in two previous publications, one on propanal (Yarnall et al. 2020) and the other on benzene (Hudson et al. 2022), and resemble the approach of Luna et al. (2012). Briefly, we grew ices on the precooled gold-coated surface of a QCM held in a UHV chamber. The increase in the microbalance's oscillator frequency was recorded as the resulting ice was slowly warmed (at 1 K minute^{-1}) to sublimation. At each time step, comparison of the observed frequency to the known frequency of a blank substrate at the same temperature gave the extent to which the observed changes were due to nitrile-ice sublimation. More specifically, with f_0 being the QCM's frequency (in hertz) with no sample present and f being the oscillator frequency with an ice on the

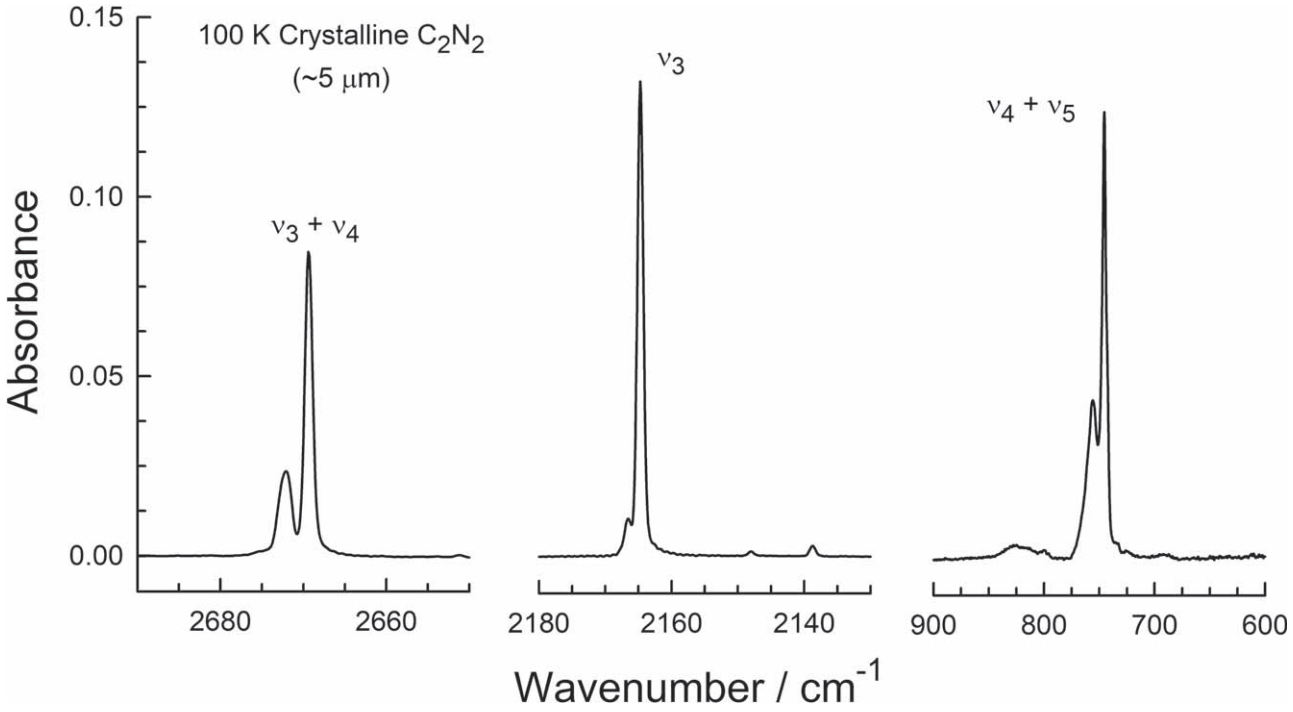

Figure 2. The three strongest features in the mid-IR spectrum of crystalline C_2N_2 deposited and recorded at 100 K. Small peaks near 2148 and 2139 cm^{-1} are from ^{15}NCCN and NC^{13}CN, respectively. A weak, broad band near 820 cm^{-1} is from HCN. The ice thickness was 4.7 μm = 4.7 × 10^{-4} cm (channel fringes removed for clarity).

substrate, then

$$\mu = \kappa\left(\frac{1}{f} - \frac{1}{f_0}\right) \quad (2)$$

gave the ice's mass per unit area (μ, in grams per square centimeter) at each temperature during a warming sequence, with $\kappa = 4.417 \times 10^5$ Hz g cm^{-2} (Lu & Lewis 1972). The flux (F) of subliming nitrile molecules was calculated from the time derivative of μ, and then vapor pressures were found from Equation (3), where m is the mass of a molecule of the nitrile ice:

$$P = F\ \sqrt{2\pi mkT}. \quad (3)$$

Readers unfamiliar with the use of Equation (3) might wish to consult a standard textbook of physical chemistry, such as that of either Chang (2000) or Atkins & de Paula (2006).

The procedure just described was followed for four HCN ices and the resulting vapor pressures averaged at temperatures (±0.1 K) from 121 to 139 K at 1 K intervals. A Clausius–Clapeyron plot (i.e., ln P as a function of $1/T$) gave a line with a slope, obtained from a least-squares fit, from which an enthalpy of sublimation, $\Delta H_{\rm subl}$, was calculated. The result was Equation (4) below, with pressure in Torr (i.e., a standard state of 1 Torr):

$$\ln(P) = (-4568)\left(\frac{1}{T}\right) + 21.61. \quad (4)$$

Units of Torr are used here to match our previous work and the older literature, but conversions to other pressure units can be made with 1 Torr = 133.322 Pa and 1 bar = 10^5 Pa; see also Tables 6 and 7 in the Appendix.

Table 3
Results for Selected IR Features of Crystalline C_2N_2 at 100 K[a]

Assignment	$\tilde{\nu}$/cm^{-1}	Integration Range/cm^{-1}	$A'/10^{-18}$ cm molecule^{-1}
$\nu_3 + \nu_4$	2669	2680–2662	0.056
ν_3	2165	2170–2160	0.058
$\nu_4 + \nu_5$	745	780–720	0.430

Note.
[a] See the text for comments on uncertainties in A' values.

The first term in parentheses on the right-hand side of Equation (4) equals $-\Delta H_{\rm subl}/R$, where R is the ideal gas constant (8.31446 × 10^{-3} kJ K^{-1} mol^{-1}). This gave $\Delta H_{\rm subl} = 37.98 \pm 0.03$ kJ mol^{-1} for crystalline HCN. The literature result is 35.6 kJ mol^{-1} based on data from ~240 to 260 K (Stull 1947).

Work similar to that just described was carried out with four cyanogen ices. The Clausius–Clapeyron equation obtained was Equation (5) below, from which $\Delta H_{\rm subl} = 36.02 \pm 0.03$ kJ mol^{-1} was derived. The literature result for C_2N_2 ice is 33.6 kJ mol^{-1} from measurements at ~180–250 K (Stull 1947):

$$\ln(P) = (-4333)\left(\frac{1}{T}\right) + 23.95. \quad (5)$$

We note that the difference in $\Delta H_{\rm subl}$ values for our nitriles is about 2 kJ mol^{-1}, with the HCN value being the higher, compared to the same order, the same difference, and similar values in the compilation of Stull (1947).

Our vapor pressures for HCN and C_2N_2 are given in Tables 4 and 5 and in the lower-left corner of each panel of Figure 5. We have connected our low-temperature results to the higher-temperature values in the literature for HCN and C_2N_2 by using

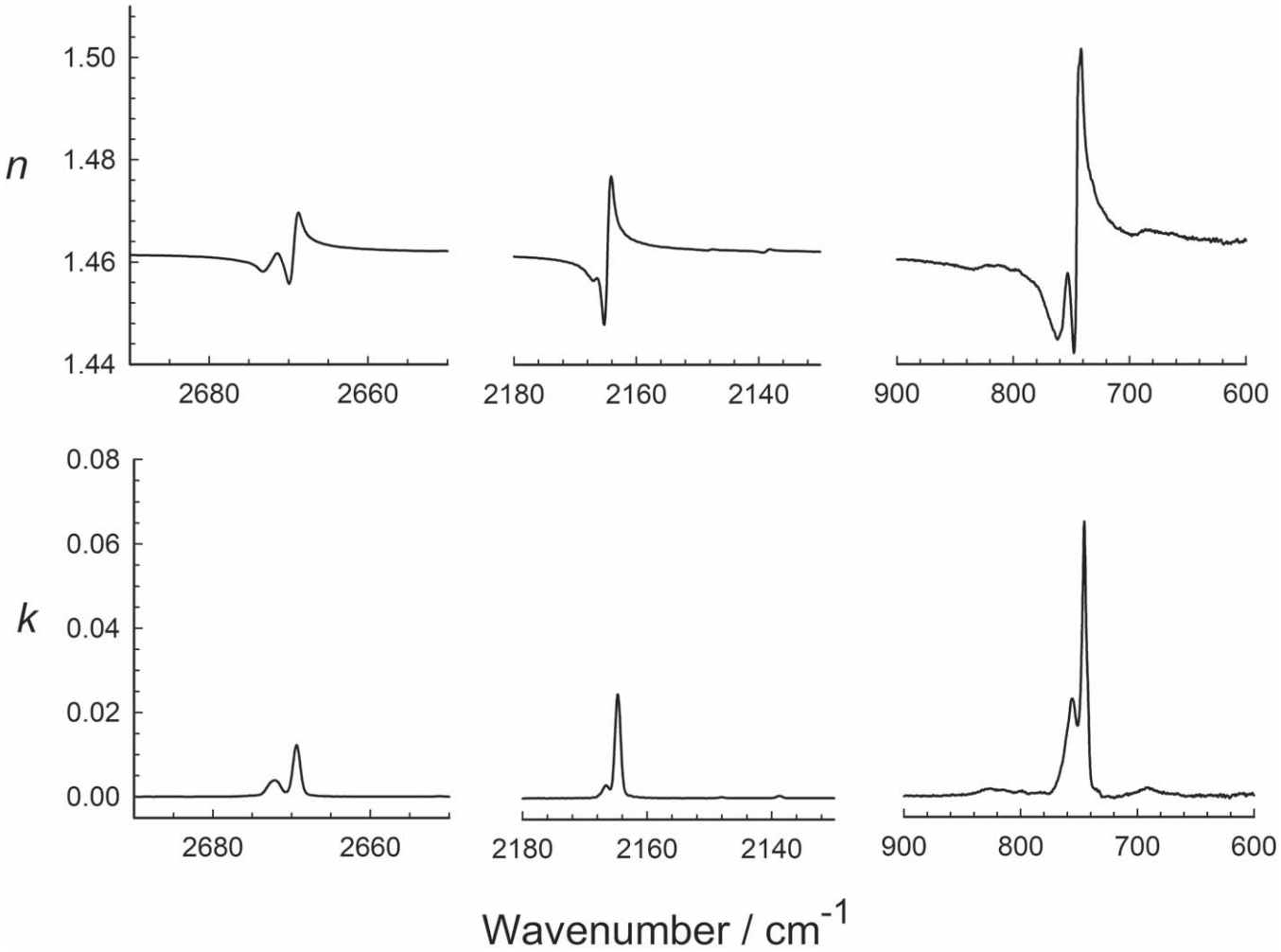

Figure 3. Optical constants for crystalline cyanogen at 100 K. The three regions are the same as in Figure 2.

the Cox equation, which has the form

$$\ln \frac{P}{P_0} = \left(1 - \frac{T_0}{T}\right) \exp\left(A_0 + A_1 T + A_2 T^2\right), \quad (6)$$

where T_0 and P_0 are triple-point values (Cox 1936). The A_i values were found by least-squares fits of Equation (6) to our data and the data in the literature. For HCN, we obtained $A_0 = 2.560$, $A_1 = 4.728 \times 10^{-3}$ K^{-1}, and $A_2 = -1.521 \times 10^{-5}$ K^{-2}, with $T_0 = 259.86$ K and $P_0 = 140.83$ Torr. For C_2N_2, we found $A_0 = 2.8927$, $A_1 = -4.6951 \times 10^{-4}$ K^{-1}, and $A_2 = -5.2032 \times 10^{-7}$ K^{-2}, with $T_0 = 245.32$ K and $P_0 = 563.30$ Torr. NIST's Chemistry WebBook was the source for the C_2N_2 triple-point values.[1] The HCN triple-point data is from Giauque & Ruehrwein (1939).

The vapor pressures in the second column of Tables 4 and 5 were found from the Clausius–Clapeyron fits to the data for HCN and C_2N_2 (Equations (4) and (5), respectively). A variation of ±0.1 K for our measured temperatures can lead to systematic uncertainties in these pressures, which we evaluated by finding the maximum and minimum pressures in the Clausius–Clapeyron fits for a 0.2 K window centered on the temperature for which each pressure is reported. The final vapor-pressure uncertainties are 3%–4% for the temperatures listed in Tables 4 and 5, with the higher uncertainty at the lower temperatures of Table 5 for C_2N_2.

[1] Accessible online at http://webbook.nist.gov/chemistry/.

4. Discussion

4.1. Densities and Refractive Indices

The density and refractive index of crystalline HCN have been discussed previously (Gerakines et al. 2022), so here we consider only results for C_2N_2. Suffice it to say that our density of $\rho = 1.186$ g cm^{-3} compares favorably with an earlier value of 1.25 g cm^{-3} from a diffraction measurement, with the crystalline ice grown by a different method (Parkes & Hughes 1963). Our $n_{670} = 1.462$ is slightly higher than that of Moore et al. (2010), 1.42 at 90 K. A value of ∼1.37 ± 0.07 was estimated by Ospina et al. (1988), but few details were provided, such as the temperature and the number of measurements.

Another way to evaluate our n and ρ results for C_2N_2 is to calculate the molecule's polarizability (α) using Equation (7):

$$\frac{4\pi}{3} N_A \alpha = \frac{M}{\rho} \frac{n^2 - 1}{n^2 + 2}. \quad (7)$$

Our n and ρ values for cyanogen give $\alpha = 4.85$ Å^3, within about 3% of the 5.02 Å^3 value of Hirschfelder et al. (1954). In contrast, combining the n values of Moore et al. (2010) and Ospina et al. (1988) with the ρ from diffraction work gives

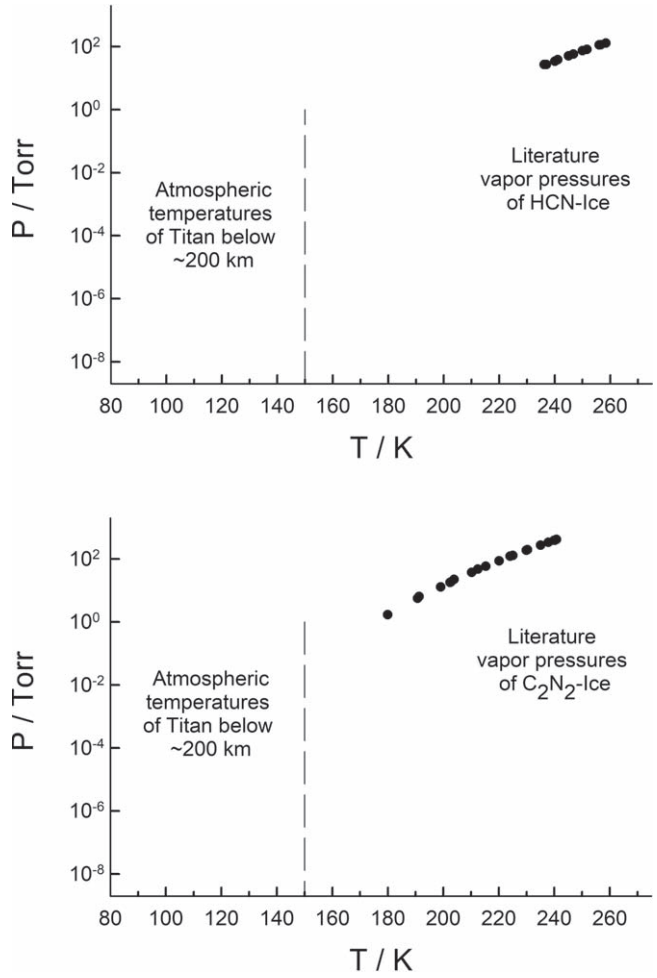

Figure 4. Vapor pressures of crystalline HCN and crystalline C_2N_2 from the literature. In the upper panel, six data points of Lewis & Schutz (1934) have been plotted, along with values at six temperatures from the vapor-pressure curve of Appleton & Van Hook (1982); see the text for sources of data for C_2N_2.

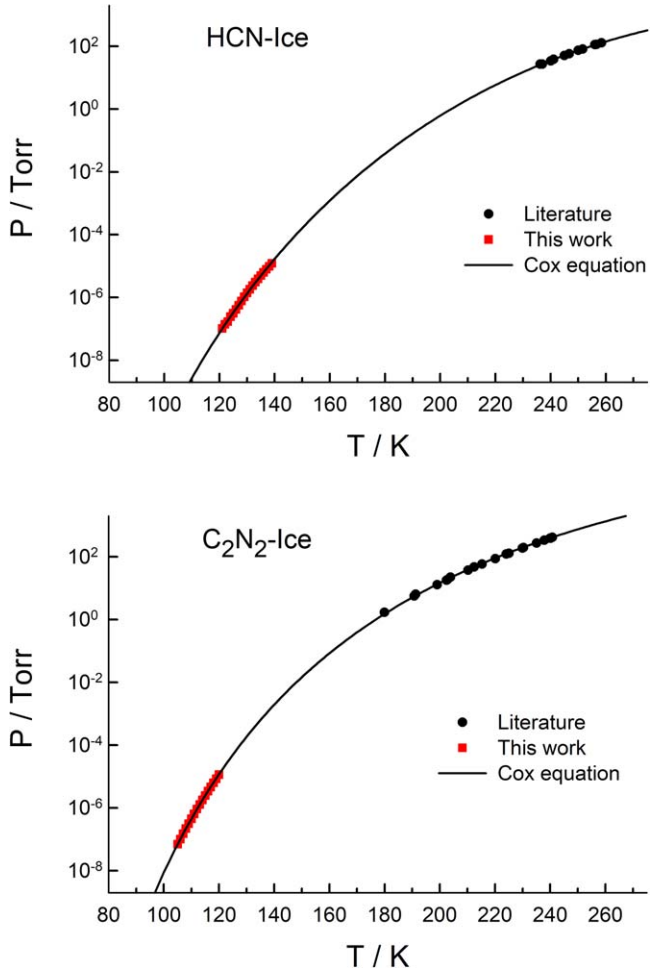

Figure 5. Vapor pressures of crystalline HCN and crystalline C_2N_2 from the literature results and from the present work. The high- and low-temperature data in each panel are connected with a smooth curve, the Cox equation.

differences of about 17% and 26%, respectively, from this same 5.02 Å^3.

4.2. Infrared Spectra of Ices

As with the n_{670} and ρ of crystalline HCN, that ice's IR spectrum was discussed by Gerakines et al. (2022), so here we focus on C_2N_2. The weakness of cyanogen's mid-IR features already has been mentioned, an observation made earlier by Verderame et al. (1963). Those authors, and later Ospina et al. (1988) and Dello Russo & Khanna (1996), published IR spectra of crystalline C_2N_2, but on such small scales that direct visual comparisons are difficult. Qualitatively, our spectrum of crystalline C_2N_2 resembles that of Verderame et al. (1963) at 80 K. Peak positions in those same authors' Table 1 are within about 1 cm^{-1} of our own and clearly indicate a small side peak for each of the three large bands of our Figure 2. Verderame et al. (1963) also show the same two features that we found for the band near 2165 cm^{-1}, and with the same separation within those authors' stated uncertainty of 0.5 cm^{-1} with a dispersive spectrometer. We also observed weak isotopic features (e.g., 2148 cm^{-1} for ^{15}NCCN and 2139 cm^{-1} for NC^{13}CN) reported by Verderame et al. (1963). With our highest resolution, 0.125 cm^{-1}, we were just able to discern an additional splitting in the ν_3 peak of Figure 2, confirming the small splitting reported by Verderame & Nixon (1965), apparently for the first time. We conclude from these largely qualitative observations that the crystalline C_2N_2 ices we studied were essentially identical in nature to those in the relevant spectroscopic literature.

Of the previous publications on IR spectra of crystalline C_2N_2, only the papers of Ospina et al. (1988) and Dello Russo & Khanna (1996) provide ice thickness, numerical scales, band strengths, and spectral resolution needed for quantitative comparisons. However, a difference in refractive indices to calculate ice thicknesses makes a direct comparison difficult. Ospina et al. (1988) reported an estimate of n, but few details were provided. From the estimated n, ice thicknesses were determined with channel fringes, but the spectrum shown possesses a very irregular fringe pattern, which introduces considerable uncertainty into thickness measurements and thus band strengths.

A second obstacle to making quantitative intensity comparisons to the papers of Ospina et al. (1988) and Dello Russo & Khanna (1996) is those papers' lack of integration ranges. Without such limits it is impossible to know if both the large and small components in our Figure 2 were integrated in the

Table 4
Vapor Pressures of Crystalline HCN[a]

T/K	Average[b] $P/10^{-6}$ Torr	Cox Equation $P/10^{-6}$ Torr	Fray & Schmitt[c] $P/10^{-6}$ Torr
121	0.10	0.10	0.20
122	0.14	0.14	0.28
123	0.17	0.18	0.38
124	0.24	0.25	0.53
125	0.32	0.33	0.71
126	0.42	0.44	0.97
127	0.57	0.58	1.30
128	0.77	0.77	1.74
129	1.05	1.01	2.33
130	1.40	1.33	3.09
131	1.82	1.74	4.08
132	2.38	2.27	5.37
133	3.07	2.95	7.03
134	3.94	3.82	9.17
135	5.01	4.93	11.91
136	6.31	6.35	15.41
137	7.91	8.14	19.86
138	9.83	10.42	25.50
139	12.21	13.30	32.61

Notes.
[a] Vapor pressures rounded to two decimal places. Values at temperatures not listed can be found by using Equation (6). Vapor-pressure uncertainties are 3%–4%.
[b] Pressures in this column represent the average over a range covering ±0.1 K of the temperature listed. For example, the pressure listed at 121 K covers data from 120.9 to 121.1 K.
[c] Vapor pressures of HCN in this column were calculated with the equation proposed by Fray & Schmitt (2009).

Table 5
Vapor Pressures of Crystalline C_2N_2[a]

T/K	Average[b] $P/10^{-6}$ Torr	Cox Equation $P/10^{-6}$ Torr	Fray & Schmitt[c] $P/10^{-6}$ Torr
105	0.070	0.070	0.11
106	0.10	0.10	0.17
107	0.15	0.15	0.24
108	0.22	0.22	0.34
109	0.31	0.31	0.48
110	0.45	0.45	0.68
111	0.64	0.64	0.95
112	0.92	0.91	1.32
113	1.30	1.28	1.83
114	1.80	1.79	2.51
115	2.49	2.49	3.44
116	3.43	3.44	4.68
117	4.64	4.72	6.33
118	6.29	6.45	8.53
119	8.49	8.76	11.43
120	11.46	11.85	15.24

Notes.
[a] Vapor pressures rounded to two decimal places, except in the first row. Values at temperatures not listed can be found by using Equation (6). Vapor-pressure uncertainties are 3%–4%.
[b] Pressures in this column represent the average over a range covering ±0.1 K of the temperature listed. For example, the pressure listed at 105 K covers data from 104.9 to 105.1 K.
[c] Vapor pressures of C_2N_2 in this column were calculated with the equation proposed by Fray & Schmitt (2009).

earlier papers or if only the areas of the larger bands were measured.

Little more can be said in relation to the earlier work of Ospina et al. (1988) and Dello Russo & Khanna (1996) except that the $\nu_3 + \nu_4$ and ν_3 IR bands in their spectra have about the same integrated intensities, as do ours, and that the $\nu_4 + \nu_5$ feature is about 5 times stronger, in rough agreement with our work. These are not comparisons on an absolute scale, yet relative intensities are still valuable as they permit scaling to unmeasured IR features. For example, the far-IR band of C_2N_2 near 244 cm^{-1} was found by Khanna and colleagues to be about 28 times more intense than the strong $\nu_4 + \nu_5$ feature we measured at 745 cm^{-1}. From our Table 3, we can estimate that $A'(244\ cm^{-1}) \approx 28 \times 0.430 \times 10^{-18}$ cm molecule^{-1} $= 1.2 \times 10^{-17}$ cm molecule^{-1}.

We know of only two other sets of IR optical constants for cyanogen with which to compare our $n(\tilde{\nu})$ and $k(\tilde{\nu})$ results of Figure 3. Our value of $k(745\ cm^{-1})$ at 100 K and 1 cm^{-1} resolution is just over twice that of Moore et al. (2010), who used a lower resolution (2 cm^{-1}) and temperature (95 K), and similar comments apply to other IR peaks. The C_2N_2 ice of Moore et al. (2010) was made at 20 K as an amorphous solid and then warmed to induce crystallization, which might explain some of the differences in spectra and optical constants. There is also the possibility that the crystallization was incomplete after that warming, although none of the nominally forbidden IR bands seem to be present (i.e., the Raman allowed features of our Table 2). Little more can be said without additional work.

Ospina et al. (1988) showed mid-IR optical constants for crystalline C_2N_2, but the figure published is so small that precise comparisons to our work are difficult. The tallest mid-IR peak has $k(745\ cm^{-1}) \approx 0.040$ at 70 K, while we find $k(745\ cm^{-1}) \approx 0.065$ at 100 K. It is possible, as with the case of Moore et al. (2010), that amorphous ice is present in the C_2N_2 sample of Ospina et al. (1988) due to the lower deposition temperature, but more work is needed to test this possibility. Differences in computational methods also might explain the differences in $k(745\ cm^{-1})$. Differences in $n(\tilde{\nu})$ seem mainly due to the different choices of a reference refractive index.

4.3. Vapor Pressures of Ices

There are no published vapor pressures available for comparison to our results for HCN and C_2N_2 ices at ~100 to 140 K. However, comparisons can be made to results extrapolated from higher temperatures. Fray & Schmitt (2009) reviewed vapor-pressure data in the literature for our two compounds and suggested equations for extrapolating. The comparisons are easily summarized:

1. For crystalline HCN, the five-term equation of Fray & Schmitt (2009) leads to vapor pressures from about 120 to 140 K that are about 130% too high when compared to our measured values. Our version of the Cox equation, seen in the upper panel of Figure 5, leads to an average deviation of about 4%.
2. For crystalline C_2N_2, the two-term Clapeyron equation of Fray & Schmitt (2009) leads to vapor pressures from 105 to 120 K that are about 45% too high when compared to our measured values, while our version of the Cox equation, seen in the lower panel of Figure 5, leads to an average deviation of about 1%.

We recommend that the equations we have proposed for HCN and C_2N_2 vapor pressures be used in the future unless percent differences on the order of 50%–100% can be tolerated.

4.4. Applications and Future Work

Perhaps the parts of our work that are most directly applicable to planetary science is that (i) we have measured HCN and C_2N_2 vapor pressures at lower temperatures than before, and (ii) we have found those pressures to be slightly lower than expected when compared to extrapolations of published results. This implies that the condensation of these two gases to make crystalline ices in Titan's atmosphere will occur at slightly higher altitudes than stated in the literature, although the difference probably is not great. Extensions to other compounds of the vapor-pressure measurements described here are desirable.

Beyond vapor pressures, our new n and ρ values for crystalline C_2N_2 will be useful in future work on this compound, such as the preparation of ices of known composition. We recently published examples of how n, ρ, and band strengths can be useful in making ice mixtures of very precise composition (Yarnall & Hudson et al. 2022), which could be extended to mixtures with cyanogen. Similarly, our band strengths can be used to make cyanogen ices of known column density (or thickness) so that quantitative measurements of photolytic or radiolytic yields, for example, can be carried out.

Qualitatively, our IR spectra of HCN and C_2N_2 are as expected from earlier work on these compounds. What is new is that we have reported band strengths with specific integration limits, have checked for resolution limitations, and have measured both n and ρ for our ices. All of these tasks lead to the best mid-IR band strengths for crystalline HCN and C_2N_2 now available for these compounds, A' values that can be adopted as reference values for studies at temperatures and wavenumbers (or wavelengths) other than those we have used. It is easy to conceive of future investigations that cover these variables.

As a final comment, we note that cyanogen (:N≡C-C≡N:) has the same NCC arrangement of atoms as amino acids. One can envision the possibility of reduction of one of the molecule's C≡N triple bonds to give aminoacetonitrile, followed by hydrolysis to give glycine, as in the sequence shown below:

$$:N\equiv C-C\equiv N: \rightarrow H_2N-CH_2-C\equiv N:$$
$$\rightarrow H_2N-CH_2-COOH.$$

We are not aware of laboratory investigations of these changes in ices.

5. Conclusions

Infrared band strengths for crystalline C_2N_2 have been newly measured and the results presented, along with new measurements of the underlying physical properties, n and ρ, on which band strength determinations rest. The IR spectra previously published for solid C_2N_2 have been verified qualitatively, even the small solid-state splittings and isotopic features. There is at least rough quantitative agreement with previous reports of IR intensities, but the lack of integration limits and uncertain n and ρ values in earlier work hinders close comparisons.

Vapor pressures for crystalline HCN and C_2N_2 are reported here for lower temperatures than in earlier work, temperatures relevant to Titan's atmosphere. The lower values of the new vapor pressures, compared to those obtained from extrapolations of higher-temperature work, shift the condensation of these compounds to slightly higher Titan altitudes. Future work will determine the size of the change.

Acknowledgments

This work was supported by the Planetary Science Division Internal Scientist Funding Program through the Fundamental Laboratory Research (FLaRe) work package at the NASA Goddard Space Flight Center. Assistance also was provided through the Goddard Center for Astrobiology and the NASA Astrobiology Institute.

Appendix

Tables 6 and 7 show the vapor pressures of HCN and C_2N_2, respectively, in three sets of units.

Table 6
Vapor Pressures of Crystalline HCN

T/K	Average[a,b] $P/10^{-6}$ Torr	Average[c] $P/10^{-6}$ Pa	Average[c] $P/10^{-9}$ bar
121	0.10	14	0.14
122	0.14	19	0.19
123	0.17	23	0.23
124	0.24	33	0.33
125	0.32	42	0.42
126	0.42	56	0.56
127	0.57	75	0.75
128	0.77	103	1.03
129	1.05	140	1.40
130	1.40	187	1.87
131	1.82	243	2.43
132	2.38	317	3.17
133	3.07	409	4.09
134	3.94	525	5.25
135	5.01	668	6.68
136	6.31	842	8.42
137	7.91	1060	10.60
138	9.83	1310	13.11
139	12.21	1627	16.27

Notes.
[a] Vapor pressures rounded to two decimal places. Values at temperatures not listed can be found by using Equation (6). Vapor-pressure uncertainties are 3%–4%.
[b] Pressures in this column represent the average over a range covering ±0.1 K of the temperature listed. For example, the pressure listed at 121 K covers data from 120.9 to 121.1 K.
[c] Vapor pressures calculated from column (2) using 1 Torr = 133.322 Pa and 1 bar = 10^5 Pa.

Table 7
Vapor Pressures of Crystalline C_2N_2

T/K	Average[a,b] $P/10^{-6}$ Torr	Average[c] $P/10^{-6}$ Pa	Average[c] $P/10^{-9}$ bar
105	0.070	9	0.09
106	0.10	14	0.14
107	0.15	20	0.20
108	0.22	29	0.29
109	0.31	42	0.42
110	0.45	60	0.60
111	0.64	86	0.86
112	0.92	120	1.20
113	1.30	173	1.73
114	1.80	240	2.40
115	2.49	332	3.32
116	3.43	457	4.57
117	4.64	619	6.19
118	6.29	838	8.38
119	8.49	1130	11.30
120	11.46	1527	15.27

Notes.
[a] Vapor pressures rounded to two decimal places, except in the first row. Values at temperatures not listed can be found by using Equation (6). Vapor-pressure uncertainties are 3%–4%.
[b] Pressures in this column represent the average over a range covering ± 0.1 K of the temperature listed. For example, the pressure listed at 105 K covers data from 104.9 to 105.1 K.
[c] Vapor pressures calculated from column (2) using 1 Torr = 133.322 Pa and 1 bar = 10^5 Pa.

ORCID iDs

Reggie L. Hudson https://orcid.org/0000-0003-0519-9429
Perry A. Gerakines https://orcid.org/0000-0002-9667-5904

References

Agúndez, M., Cernicharo, J., de Vicente, P., et al. 2015, A&A, 579, L10
Anderson, C. M., Samuelson, R. M., & Nna-Mvondo, D. 2018, SSRv, 214, 125
Andrews, B., Anderson, A., & Torrie, B. 1984, JRSp, 15, 67
Appleton, G. T., & Van Hook, W. A. 1982, J. Chem. Eng. Ref. Data, 27, 363
Atkins, P., & de Paula, J. 2006, Physical Chemistry (8th ed.; New York: Freeman), 457
Bézard, B., Vinatier, S., & Achterberg, R. K. 2018, Icar, 302, 437
Chang, R. 2000, Physical Chemistry for the Chemical and Biological Sciences (Sausalito, CA: Univ. Science Books), 56
Coustenis, A., Schmitt, B., Khanna, R. K., & Trotta, F. 1999, P&SS, 47, 1305
Cox, E. R. 1936, J. Ind. Eng. Chem., 28, 613
Dello Russo, N., & Khanna, R. K. 1996, Icar, 123, 366
Fray, N., & Schmitt, B. 2009, P&SS, 57, 2053
Gerakines, P. A., & Hudson, R. L. 2015, ApJL, 808, L40
Gerakines, P. A., & Hudson, R. L. 2020, ApJ, 901, 1
Gerakines, P. A., Moore, M. H., & Hudson, R. L. 2004, Icar, 170, 204
Gerakines, P. A., Yarnall, Y. Y., & Hudson, R. L. 2022, MNRAS, 509, 3515
Giauque, W. F., & Ruehrwein, R. A. 1939, JAChS, 61, 2626
Griffiths, P. R., & de Haseth, J. A. 1986, Fourier Transform Infrared Spectrometry (New York: Wiley), 350
Hänni, N., Altwegg, K., Balsiger, H., Combi, M., et al. 2021, A&A, 647, A22
Harrick, N. J. 1971, ApOpt, 10, 2344
Hirschfelder, J. O., Curtiss, C. F., & Bird, R. B. 1954, Molecular Theory of Gases and Liquids (New York: Wiley), 950
Hollenberg, J. L., & Dows, D. A. 1961, JChPh, 34, 1061
Hudson, R. L. 2020, Icar, 338, 113548
Hudson, R. L., Loeffler, M. J., Ferrante, R. F., Gerakines, P. A., & Coleman, F. M. 2020, ApJ, 891, 22
Hudson, R. L., Yarnall, Y. Y., & Gerakines, P. A. 2022, PSJ, 3, 120
Irvin, J. A., & Quickenden, T. I. 1983, JChEd, 60, 711
Khanna, R. K., Perera-Jarmer, M. A., & Ospina, M. J. 1987, Spec. Acta, 43A, 421
Kunde, V. G., Aikin, A. C., Hanel, R. A., Jennings, D. E., et al. 1981, Natur, 292, 686
Lai, J. C.-Y., Cordiner, M. A., Nixon, C. A., Achterberg, R. K., et al. 2017, AJ, 154, 206
Lewis, G. N., & Schutz, P. W. 1934, JAChS, 56, 1002
Loomis, R. A., Burkhardt, A. M., Shingledecker, C. N., et al. 2021, NatAs, 5, 188
Lovas, F. J., Hollis, J. M., Remijan, A. J., & Jewell, P. R. 2006, ApJL, 645, L137
Lu, C. S., & Lewis, O. 1972, JAP, 43, 4385
Luna, R., Millan, C., Domingo, M., Santonja, C., & Satorre, M. 2012, Vacuu, 86, 1969
McGuire, B. A., Burkhardt, A. M., & Kalenskii, S. 2018, Sci, 359, 202
McGuire, B. A., Burkhardt, A. M., Loomis, R. A., Shingledecker, C. N., et al. 2020, ApJL, 900, L10
Moore, M. H., Ferrante, R. F., Moore, W. J., & Hudson, R. L. 2010, ApJS, 191, 96
Ospina, M., Zhao, G., & Khanna, R. K. 1988, Spec. Acta, 44A, 23
Parkes, A. S., & Hughes, R. E. 1963, Acta Cryst., 16, 734
Perry, J. H., & Bardwell, D. C. 1925, JAChS, 47, 2629
Press, W. H., Teukolsky, S. A., Vetterline, W. T., & Flannery, B. P. 1992, Numerical Recipes in FORTRAN (2nd ed.; Cambridge: Cambridge Univ. Press), 660
Ruehrwein, R. A., & Giauque, W. F. 1939, JAChS, 61, 2940
Sagan, C., & Thompson, W. R. 1984, Icar, 59, 133
Shimanouchi, T. 1972, JPCRD, 6, 993
Sita, M. L., Changala, P. B., Xue, C., et al. 2022, ApJL, 938, L12
Soifer, B. T., Puetter, R. C., Russell, R. W., et al. 1979, ApJ, 232, L53
Stull, D. R. 1947, Ind. Eng. Chem., 39, 517
Tempelmeyer, K. E., & Mills, D. W. 1968, JAP, 39, 2968
Verderame, F. D., Nebgen, J. W., & Nixon, E. R. 1963, JChPh, 39, 2274
Verderame, F. D., & Nixon, E. R. 1965, JChPh, 42, 3337
Yarnall, Y. Y., Gerakines, P. A., & Hudson, R. L. 2020, MNRAS, 494, 4606
Yarnall, Y. Y., & Hudson, R. L. 2022, ApJL, 91, L4